Validation of the 4C Code on the AC Loss Tests of a Full-Scale ITER Coil

A New Efficient Mirror Cooling for the Transmission Line of Fusion Reactor ECH Systems Based on Triply Periodic Minimal Surfaces

Eleonora Gajetti, Massimiliano Bonesso, Alessandro Bruschi, Francesco Fanale, Saul Garavaglia, Gustavo Granucci, Alessandro Moro, Adriano Pepato, Afra Romano, and Laura Savoldi, *Member, IEEE*

***Abstract*— An innovative cooling strategy for the mirrors of the transmission line of the electron cyclotron heating (ECH) of a fusion research reactor, the divertor tokamak test (DTT) facility, is presented and investigated here based on triply periodic minimal surfaces (TPMSs). After the check on the manufacturability of gyroid and Split-P lattices of unit cell size ranging from 3 to 8 mm, extensive numerical investigations by conjugate heat transfer analyses have been performed. The heat removal capability has been assessed together with the pressure drop for all heat sinks. The temperature field in the mirror has been evaluated and used for the assessment of the deformation of the mirror reflective surface. The results show that all tested TPMSs are highly efficient in the heat removal, with low hotspot temperatures, minimal pressure drop, and low deformation of the reflective surface.**

***Index Terms*— Cooling, fusion reactor design, microwave generation, mirrors, transmission line.**

I. Introduction

IN THE electron cyclotron heating (ECH) system for fusion devices [1], the transmission of MW-level microwave beams routed from gyrotrons [2] to the plasma chamber typically involves several mirrors. In the divertor tokamak test (DTT) facility [3], [4], the ECH system, currently under design [5], [6], shall provide auxiliary heating power to the plasma by means of 32-MW-class gyrotrons [7] operating at 170 GHz (as those foreseen for ITER [8], [9], [10], [11]), long quasi-optical transmission lines enclosed in pipes under vacuum [12], and front-steering antennae composed of identical modular units of two mirrors [13]. The gyrotrons are grouped in four clusters of eight sources each: the power of a cluster is transmitted by a quasi-optical evacuated multibeam transmission line [14] up to two launchers in the DTT equatorial and upper ports, where the beams are launched into the plasma by independently steerable mirror antennas.

During the beam reflection, ohmic losses are produced in the conductive material, resulting in a large heat load on the mirrors surface, eventually coupled to a nuclear load coming from the plasma chamber [15]. In order to prevent the deformation of the mirrors from their ideal shape, they need to be cooled actively through pressurized subcooled water. Typically, the cooling is achieved through cooling channels (following an S-shaped trajectory in the case of the launcher mirrors in EAST [16] and KSTAR [17] or a spiral trajectory in W7-X [18] and in some launcher mirrors for ITER [19], [20], [21], while others rely on serpentine cooling [22], [23]). More recently, new designs have been introduced, as in [24] for instance, where the heat sink is based on cylindrical pins around which the coolant is free to move without any predefined channel, homogenizing the temperature of the mirror. Moreover, the use of additive manufacturing (AM) for the definition of innovative cooling patterns on the nonreflective side of the mirrors has been investigated in [25], showing the potentialities in terms of weight reduction.

This article aims at developing new efficient cooling systems for the ECRH mirrors, based on triply periodic minimal surfaces (TPMSs), which are excellent structures to enhance heat transfer in view of their high surface-to-volume ratio and low weight [26]. The feature of minimal surfaces implies that they have a null mean curvature in all locations, leading to low stress concentration [27]. Moreover, their structure is self-supporting, with a high stiffness [26]. The TMPS lattices, already known since the 19th century [28], are becoming more and more popular because their manufacture has been allowed by the boost of AM. Their excellent performance

Manuscript received 2 October 2023; revised 30 January 2024; accepted 7 February 2024. This work was supported in part by DTT Consortium. The review of this article was arranged by Senior Editor R. Chapman. *(Corresponding author: Laura Savoldi.)*

Eleonora Gajetti and Laura Savoldi are with the MAHTEP Group, Dipartimento Energia "Galileo Ferraris," Politecnico di Torino, 10129 Turin, Italy (e-mail: eleonora.gajetti@polito.it; laura.savoldi@polito.it).

Massimiliano Bonesso and Adriano Pepato are with the Padua Division, National Institute for Nuclear Physics, 35131 Padua, Italy (e-mail: massimiliano.bonesso@pd.infn.it; adriano.pepato@pd.infn.it).

Alessandro Bruschi, Saul Garavaglia, Gustavo Granucci, and Alessandro Moro are with the Institute for Plasma Science and Technology, National Research Council (ISTP-CNR), 20125 Milan, Italy (e-mail: alessandro.bruschi@istp.cnr.it; saul.garavaglia@istp.cnr.it; gustavo.granucci@istp.cnr.it; alessandro.moro@istp.cnr.it).

Francesco Fanale and Afra Romano are with the Fusion and Nuclear Safety Department, ENEA, 00044 Frascati, Italy, and also with DTT S.C. a r.l., 00044 Frascati, Italy (e-mail: francesco.fanale@enea.it; afra.romano@enea.it).

Color versions of one or more figures in this article are available at https://doi.org/10.1109/TPS.2024.3383275.

Digital Object Identifier 10.1109/TPS.2024.3383275

as heat sinks has been recently demonstrated by numerical investigations in [29], where different TPMS lattices, among which the gyroid and the diamond, have been analyzed and compared in detail. The simulated results have been confirmed by measurements in dedicated experiments in, e.g., [30], [31], showing better convective heat transfer performance than finned surfaces at the cost of higher flow resistance.

In this article, different TPMS lattices are being proposed and investigated for the first time as solutions for the cooling of the mirrors of the microwave transmission line of fusion machines, with particular reference to the splitter/combiner mirrors unit of the DTT facility [12]. The selected structures are the gyroid, well investigated in previous literature, and the Split-P, still not widely considered as a plausible heat sink [32]. The mirror equipped with different TPMSs is investigated parametrically considering different unit cell dimensions of the lattices, after the verification that they are printable by AM. The characterization of the thermal-hydraulic (TH) performance (in terms of hotspot and pressure drop) is conducted by means of steady-state, fully 3-D computational thermal-fluid dynamics simulations. The steady-state, thermo-mechanical (TM) analysis (maximum displacement and stress) is performed numerically by finite element analysis. The most performant lattice among the investigated ones is highlighted, analyzing at the same time the effect of the porosity on the TH and TM behavior of the cooling structure.

This article is structured as follows: first, the selected lattices are introduced, and their main features are discussed. Their application as heat sinks in the selected test case is then introduced, and the TH and TM setup for the numerical simulation is presented. Finally, the computed results are reported and widely discussed to highlight the most performant configurations for the case at hand.

II. Lattice Structures

The TPMSs are based on nonself-intersecting structures obtained by the combination of trigonometric functions in a 3-D framework. In Cartesian framework, the two structures adopted here, namely, gyroid and Split-P, are based on the following equations, where $X = (2\pi/L_{C,x})x$, $Y = (2\pi/L_{C,y})y$, and $Z = (2\pi/L_{C,z})z$:

$$\sin(X)\cos(Y) + \sin(Y)\cos(Z) + \sin(Z)\cos(X) = c \quad (1)$$

$$\begin{aligned} 1.1(&\sin(2X)\sin(Z)\cos(Y) + \sin(2Y)\sin(X)\cos(Z) \\ &+ \sin(2Z)\sin(Y)\cos(X)) - 0.2(\cos(2X)\cos(2Y) \\ &+ \cos(2Y)\cos(2Z) + \cos(2Z)\cos(2X)) \\ &- 0.4(\cos(2X)\cos(2Y)\cos(2Z)) = c. \end{aligned} \quad (2)$$

The parameters $L_{C,x}$, $L_{C,y}$, and $L_{C,z}$ control the period (i.e., the pore density) independently in the three directions. In this study, they have all been set equal to the same value L_c, which also defines the cell dimension. The parameter c controls whether the resulting structure shows more than one separate fluid regions (sheet-type) or a single fluid region (solid-type). More in detail, a solid-based structure is generated by offsetting by a certain value of c the isosurface generated by the characteristic function, while the sheet-based structure is generated by taking as the solid region the volume enclosed by the two surfaces obtained at $\pm c$. In this study, sheet and solid structures are considered for the gyroid lattice, while only the sheet structure has been considered for the Split-P lattice. The values of the parameters of (1) and (2) used for the cooling configurations investigated in this article are reported in Table I, together with the corresponding porosity Φ (computed as fluid over total volume) and wet surface-to-fluid volume S/V ratios. Sheet gyroids have been denoted as GX, solid gyroids as GY, and sheet Split-P as SX. They have all been checked to be realizable by AM, as shown in Fig. 1.

TABLE I
Geometrical Parameters of the TPMS Lattices Adopted in the Mirror Cooling

#	L_C(mm)	c	Φ	S/V (m^{-1})
GX1	3	±0.77	0.50	4.44E+3
GY2	3	0	0.50	2.90E+3
GX3	5	±0.46	0.70	2.18E+3
GY4	5	0.61	0.70	1.31E+3
GX5	8	±0.30	0.81	1.26E+3
GY6	8	0.94	0.81	7.03E+2
GY7	8	0.77	0.75	7.71E+2
GY8	8	0.62	0.70	8.27E+2
GY9	8	0.46	0.65	8.81E+2
GY10	8	0.31	0.60	9.42E+2
SX1	4	±0.70	0.49	5.11E+3
SX2	6	±0.47	0.66	2.88E+3
SX3	8	±0.37	0.74	1.99E+3

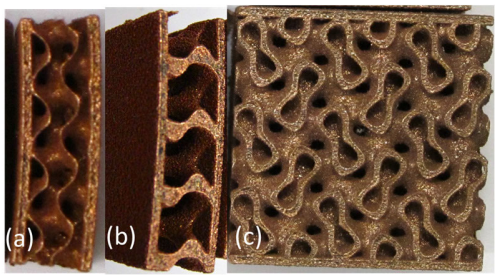

Fig. 1. Picture of a (a) sheet gyroid, (b) solid gyroid, and (c) sheet Split-P realized in CuCrZr by AM at the INFN premises in Padua, using laser powder bed fusion.

As visible in Fig. 2, the lattices with the smallest L_C show the largest surface-to-volume ratios and the smallest porosities. For a given value of L_C, the solid gyroid has the same porosity of the sheet gyroid, but a lower S/V ratio. Both lattices have lower S/V than the Split-P, but a higher porosity. If we concentrate on the solid gyroid with $L_C = 8$ mm, the decrease in the porosity related to the decrease of c (see Table I) is compensated by a small increase in the values S/V, in view of the decrease in the fluid volume for a comparable value of the surface.

Since the width of the cooling system is equal to the TPMS cell dimension, L_c, the total volume of the mirror is not the same for all the configurations. Therefore, the mirrors with TPMS with the smallest L_c, i.e., GX1, GY2, and SX1, also result in the smallest mass: 0.53-kg gyroids

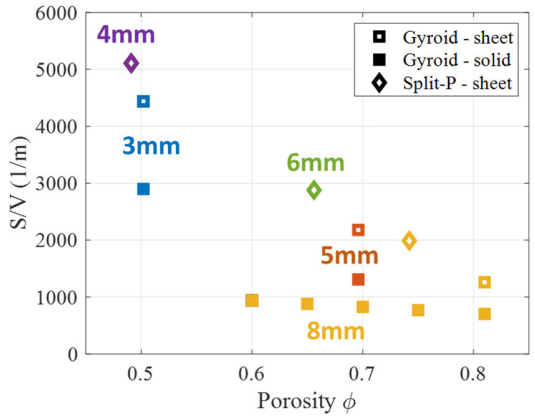

Fig. 2. Surface-to-fluid volume ratio versus porosity for the TPMS adopted in the mirror cooling. Different colors correspond to different values of L_C.

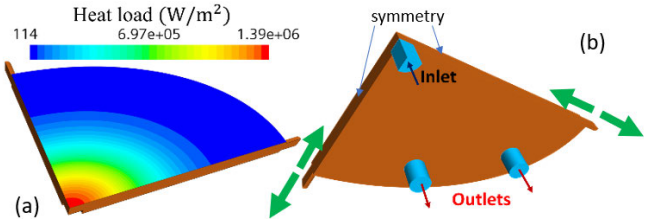

Fig. 3. Splitter mirror (a) top view, with the surface heat load, and (b) back view, with the location of the coolant inlet and outlets, and the location of the boundary conditions for the thermal-hydraulic and thermo-mechanical simulations.

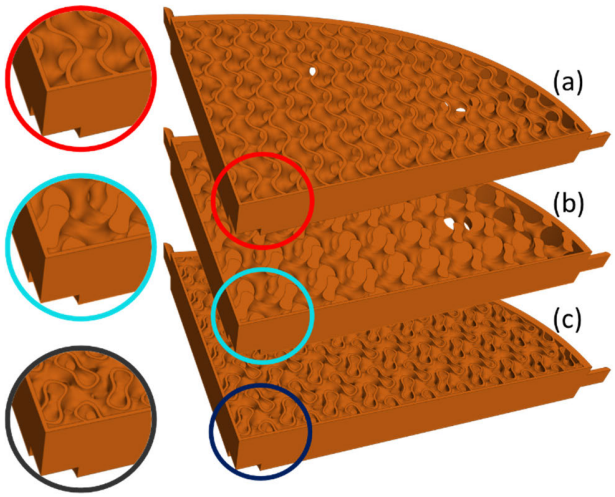

Fig. 4. Computational domain of the mirror equipped with the cooling structure (a) GX, (b) GY, and (c) SX, with zooms showing the unit cell geometry. The top heated wall has been removed here for the sake of clarity.

TABLE II
MESH PARAMETERS FOR THE GRID CONVERGENCE EVALUATION

Mesh	1 (ref)	2	3
# fluid cells	8.9M	6.7M	4.9M
# solid cells	2.7M	2.1M	1.6M
# boundary layers	10	8	6

and 0.59-kg Split-P, respectively. The reflecting layer has a constant thickness of 1 mm and its surface area is 0.013 m^2.

III. MIRROR GEOMETRY AND SIMULATION SETUP

The mirror considered here is the splitter unit of the DTT transmission line [14], with planar surface and elliptical shape with major and minor axes of 156 and 104 mm, respectively. Note that the shape and dimension have been set to intercept at least the 99.97% of the power of the beam. The mirror is to be realized in CuCrZr. Since the TPMSs are periodic but not symmetric, to decrease the computational burden, a 1-mm-width rib has been inserted along each axis, so that only 4 of the mirror can be considered in the analysis, and symmetry has been imposed on those ribs, as shown in Fig. 3. The heat load on the mirror heated surface, generated by ohmic losses due to microwave absorption, is shown in Fig. 3(a) [12]. The coolant enters from an inlet pipe located in the middle of the mirror, in correspondence of the heat flux peak value, and two outlets are designed at two different azimuthal locations [see Fig. 3(b)]. The CuCrZr domains obtained for the GX, GY e SX configurations are collected in Fig. 4. Concerning the operational conditions of the whole mirror, a flow rate of 4.2 L/min enters at 15 °C and exits at 7 bar, and the maximum achievable pressure drop is 4 bar.

In the simulations, thermal-dependent fluid properties have been chosen, following the IAPWS-IF97 standard, whereas CuCrZr properties have been provided by the TPMS manufacturers (INFN Padua [33]). The steady-state conjugate heat transfer is solved for the heat transfer between solid and fluid. The Reynolds number has been computed to be >500, value assessed to be far beyond the Darcy regime, and the $\kappa - \varepsilon$ lag elliptic-blending turbulence model has been used. Computational grids and simulations have been performed with the commercial software STAR-CCM+ [34].

For what regards the TM analysis, the temperature distribution in the solid body and the pressure field has been utilized as TM loads. Two pivots at the end of the major and minor axes may move only along their axes, as shown in Fig. 3(b). Symmetry is imposed along the minor and major axes, where the ribs have been inserted, as in the TH simulations. TM grids have been created in nTop [35] and then exported in Ansys Mechanical [36], the commercial software used for the thermomechanic simulations. Isotropic, linear, elastic behavior has been assumed. The TM analyses of Split-P structures could not be performed due to a lack of computational power.

To ensure the convergence of the TH results, three grids have been created for the GX5 lattice. The total number of cells has been risen simultaneously increasing the number of boundary layers: those parameters are shown in Table II.

The pressure drop and the maximum temperature increase have been monitored and plotted in Fig. 5: both $\Delta T_{\max}$ and Δp computed with the three grids have been normalized by the result of the finest grid (called ref in Table I). On the x-axis, in Fig. 5(a), the average cell size of the whole computational domain (Δh_{tot}) has been used, while in Fig. 5(b), the average size of the fluid domain is displayed (Δh_{fluid}). Again, Δh_{tot} and Δh_{fluid} are normalized by the reference value of the average cell sizes. The selected mesh is the second finest one, since the relative difference between the results of the finest and the second one is quite negligible, less than 0.2%. The other TPMS

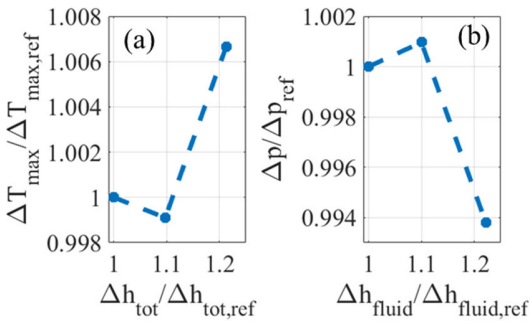

Fig. 5. Grid convergence. (a) Maximum temperature increase. (b) Pressure drop.

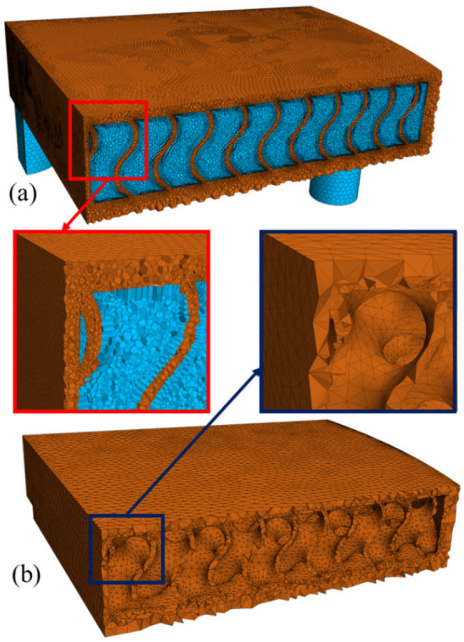

Fig. 6. Computational grids for (a) thermohydraulic simulation with finite volumes (coolant domain in light blue and solid domain in brown) and (b) thermomechanic simulation with finite elements (solid domain only).

structures have been built using the same parameters as for the second finest mesh. The adopted hexahedral mesh for the TH simulation is presented in Fig. 6(a) for the GX5 case. Note that boundary layers have been inserted to capture the near-wall behavior. The quadratic, tetrahedral mesh adopted for the same lattice in the TM simulation is displayed in Fig. 6(b).

IV. Computed Results

A. TH Performance

The flow streamlines along the TPMS structures have been drawn in Fig. 7. The sheet gyroid and the sheet Split-P induce a more intricate fluid path with respect to the solid gyroid, as expected. On the other hand, the flow complexity does not qualitatively differ in the two sheet geometries. High velocities are found only at the mirror center, where water is injected via the inlet. The mass flow rates through the two outlets have been checked to investigate the correct distribution of the fluid throughout the channels, in the GX1, GY2, and SX1 configurations. Approximately, the flow is partitioned between the two outlets by 60% (near minor axis) and 40% (near major

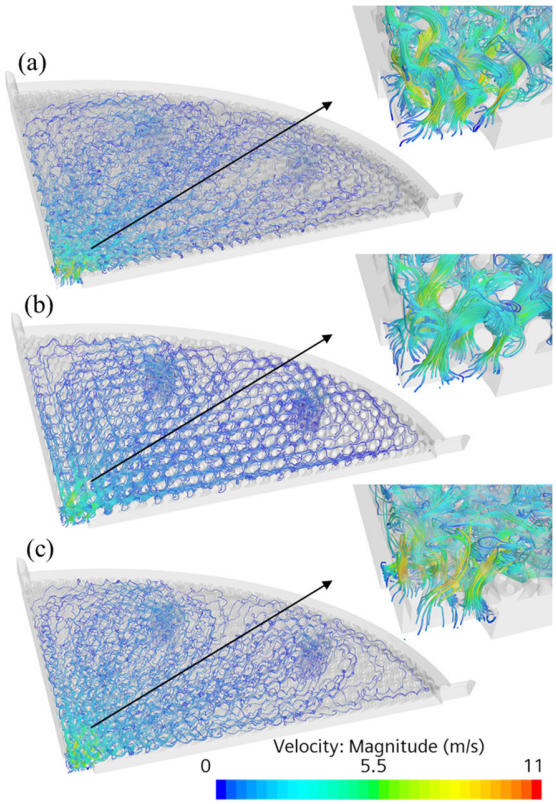

Fig. 7. Streamlines computed for the mirror equipped with the cooling structures (a) GX1, (b) GY2, and (c) SX1 colored by velocity.

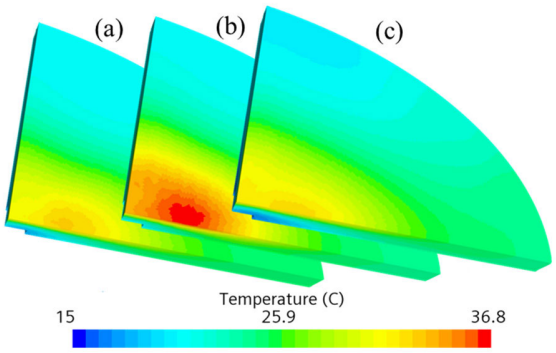

Fig. 8. Temperature map for (a) GX1, (b) GY2, and (c) SX1.

axis). Therefore, all the three systems displayed in Fig. 7 enable the fluid to distribute quite properly, with more effort toward the major axis end, where anyway the thermal load is much lower. Indeed, the combination of the TPMS cooling systems and positions of inlet/outlets performs efficiently in removing the Gaussian-shaped heat flux on the mirror layer. Yet, the nonperfect share of the flow outlets leaves some space for future improvements.

Fig. 8 presents the temperature maps on the mirror layers cooled by GX1, GY2, and SX1. The hotspot is found along the major axis, near the center of the mirror. Its location is due to the Gaussian heat load and to the lower exiting flow rate in the outlet closer to the major axis and it is independent on the TPMS structures, even at the highest porosities (∼50%).

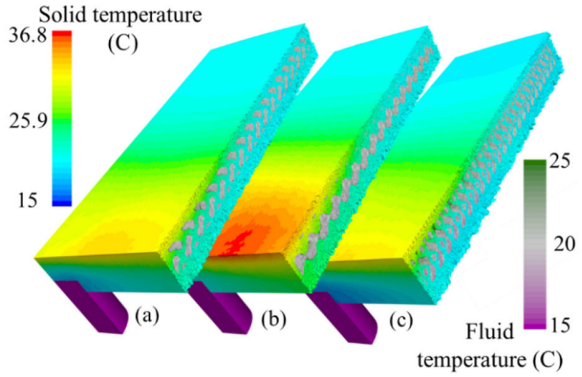

Fig. 9. Temperature map of solid and fluid domains for (a) GX1, (b) GY2, and (c) SX1.

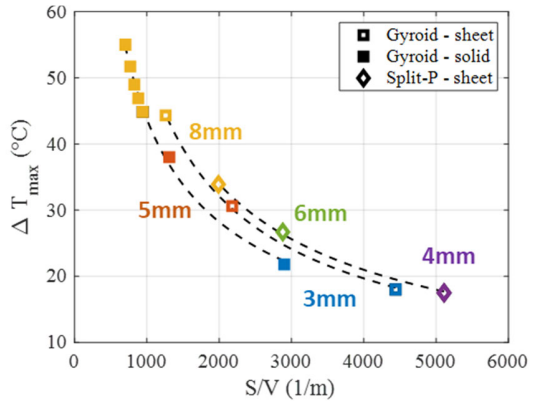

Fig. 10. Maximum temperature increase on the heated surface, computed as a function of S/V for the mirror equipped with the different TPMSs considered in this study.

The solid-G performs quite poorly compared to the sheet-G and Split-P, with 4 °C higher hotspot. The sheet gyroid and Split-P show similar results, but we should consider that the Split-P structure has been created with an $L_C = 4$ mm, whereas the tiniest gyroids have $L_C = 3$ mm. This is due to the more complicated characteristic function of the Split-P: fixing the wall thickness, gyroid structures result in lower S/V (see Table I). An insight of the fluid temperature is provided in Fig. 9. In Fig. 10, the maximum temperature increases have been correlated with the surface-to-volume ratio, which proves to be a reasonable independent parameter to characterize the TPMS heat removal capability. Indeed, Fig. 10 exhibits the strong relationship between S/V and $\Delta T_{\max}$.

To investigate and characterize the TPMS cooling system in a wide operational range, the maximum temperature increase of the mirror layer has been shown as a function of the computed pressure drop along the cooling systems in Fig. 11. As expected, increasing the L_C results in less efficient cooling systems, with higher hotspots, but lower flow impedance and thus lower pressure losses. Note that in all cases, the pressure drop is significantly lower than the constraint.

It is also important to mention that at large porosity and cell dimension, the largest contribution to the pressure loss is concentrated at the inlet. This explains why the curve in Fig. 11 has a sharp increase at low Δp.

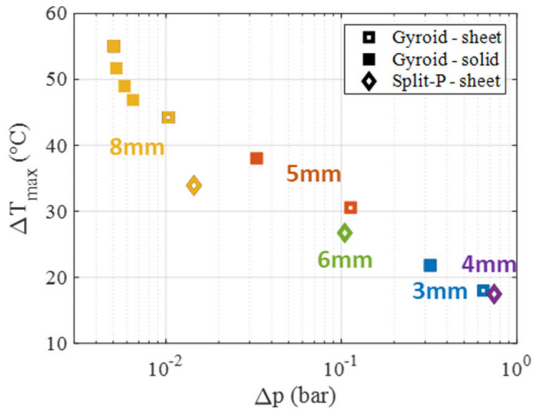

Fig. 11. TH performance computed for the mirror equipped with the different TPMSs considered in this study.

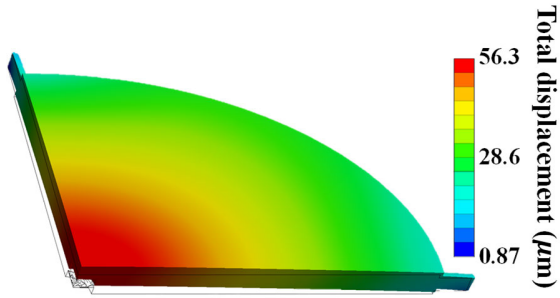

Fig. 12. Total displacement field computed for GX1.

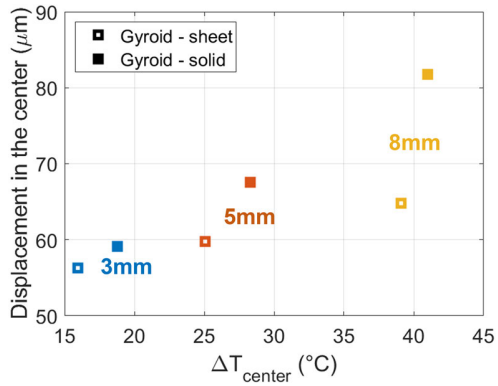

Fig. 13. Maximum displacement versus maximum temperature increase for GX1,3,5 and GY2,4,6.

B. TM Performance

Another important factor to consider in the design of innovative mirror cooling systems is the mechanical response to thermal loads. Indeed, in Fig. 12, the deformed mirror cooled with the solid-gyroid best configuration is displayed. The maximum displacement is found on the center of the mirror layer for all the configurations: this is because the center is close to the hotspot and far from the constraints. The deformation distribution follows an elliptic trend due to the mirror shape as well as the temperature distribution, in turn depending on the heat load.

The displacement values in the mirror layer center have been plotted against the temperature increase in the same location for the three solid and sheet gyroids in Fig. 13. The

relationship between temperature increase and displacement in the center is almost linear, as it might be expected because of the elastic hypothesis of the analysis. It must be noted that the stresses induced by the fluid pressure and by the thermal deformations are pretty small, being the temperature rise low as well as the overall, and local, pressure drop.

V. Conclusion and Perspective

In this article, different TPMS structures have been investigated as cooling systems for the combiner/splitter mirrors of the DTT ECH transmission line, demonstrating that gyroid and Split-P topologies can be efficiently employed as heat sinks for this application. The operational window of those structures has been widely examined by varying the cell dimension and the porosity. The current study has highlighted the dependence of the thermal performance on both the cell size and the void fraction as well as the more efficient heat removal of the sheet TPMS compared to the solid TPMS. Indeed, the TH trend of the gyroid and Split-P appears quite similar. The sheet-G geometry of 3 mm size (GX1) can achieve a maximum temperature increase equal to 18 °C with a very low pressure drop of 0.64 bar. The maximum deformation is 56.3 μm. The total mass of the mirror for this configuration is 0.53 kg of CuCrZr (considering that the surface area of the reflecting layer is 0.013 m^2). Some room for improvement remains considering that the flow rate can be incremented, without exceeding the pressure constraint, and that the fluid distribution through the two outlets might be better split. Because of the low temperature reached, corrosion should not be an issue for CuCrZr [37]. All the tested configurations have been proved to be manufacturable in small samples. The entire geometries could be printed in standard commercial 3-D metal printers because of the small mirror dimensions (156 $\times$ 104 mm).

These new heat removal systems have the potential to greatly improve the performance of the transmission line mirrors and open interesting possibilities also for the launcher mirrors, which are more challenging as they are subject to higher load and stress.

Acknowledgment

We acknowledge the CINECA award under the ISCRA initiative, for the availability of high-performance computing resources and support.

References

[1] V. Erckmann and U. Gasparino, "Electron cyclotron resonance heating and current drive in toroidal fusion plasmas," *Plasma Phys. Controlled Fusion*, vol. 36, no. 12, pp. 1869–1962, Dec. 1994.

[2] M. K. A. Thumm, G. G. Denisov, K. Sakamoto, and M. Q. Tran, "High-power gyrotrons for electron cyclotron heating and current drive," *Nucl. Fusion*, vol. 59, no. 7, Jul. 2019, Art. no. 073001.

[3] R. Albanese et al., "Design review for the Italian divertor tokamak test facility," *Fusion Eng. Des.*, vol. 146, pp. 194–197, Sep. 2019.

[4] R. Ambrosino, "DTT–divertor tokamak test facility: A testbed for DEMO," *Fusion Eng. Des.*, vol. 167, Jun. 2021, Art. no. 112330.

[5] G. Granucci et al., "The DTT device: System for heating," *Fusion Eng. Des.*, vol. 122, pp. 349–355, Nov. 2017.

[6] S. Garavaglia et al., "Progress of DTT ECRH system design," *Fusion Eng. Des.*, vol. 168, Jul. 2021, Art. no. 112678.

[7] M. Thumm, "MW gyrotron development for fusion plasma applications," *Plasma Phys. Controlled Fusion*, vol. 45, no. 12A, pp. A143–A161, Dec. 2003.

[8] K. Sakamoto et al., "Development of high power gyrotron for ITER application," in *Proc. 35th Int. Conf. Infr., Millim., THz Waves*, Sep. 2010, pp. 1–2.

[9] Z. C. Ioannidis et al., "First CW experiments with the EU ITER 1 MW, 170 GHz industrial prototype gyrotron," in *Proc. 18th Int. Vac. Electron. Conf. (IVEC)*, Apr. 2017, pp. 1–2.

[10] Z. C. Ioannidis et al., "Recent experiments with the European 1 MW, 170 GHz industrial CW and short-pulse gyrotrons for ITER," *Fusion Eng. Des.*, vol. 146, pp. 349–352, Sep. 2019.

[11] A. G. Litvak et al., "Development of 170 GHz/1 MW/50%/CW gyrotron for ITER," in *Infr. Millim. Waves, Conf. Dig. Joint 29th Int. Conf. 12th Int. Conf. THz Electron.*, 2004, pp. 111–112.

[12] A. Bruschi et al., "Conceptual design of the DTT ECRH quasi-optical transmission line," *Fusion Eng. Des.*, vol. 194, Sep. 2023, Art. no. 113727.

[13] F. Fanale et al., "Progress on the conceptual design of the antennas for the DTT ECRH system," *Fusion Eng. Des.*, vol. 192, Jul. 2023, Art. no. 113797.

[14] S. Garavaglia et al., "Development of the electron cyclotron resonance heating system for divertor tokamak test," *J. Vac. Sci. Technol. B*, vol. 41, no. 4, pp. 044201-1–044201-9, Jul. 2023.

[15] R. Villari et al., "Nuclear design of divertor tokamak test (DTT) facility," *Fusion Eng. Des.*, vol. 155, Jun. 2020, Art. no. 111551.

[16] X. Wang et al., "Research activities and progress on the long pulse ECRH launcher for EAST," in *Proc. EPJ Web Conf.*, 2019, p. 02012.

[17] M. Joung et al., "Design of ECH launcher for KSTAR advanced tokamak operation," *Fusion Eng. Des.*, vol. 151, Feb. 2020, Art. no. 111395.

[18] H. Hailer et al., "Mirror development for the 140 GHz ECRH system of the stellarator W7-X," *Fusion Eng. Des.*, vols. 66–68, pp. 639–644, Sep. 2003.

[19] M. Vagnoni, R. Chavan, M. Gagliardi, T. Goodman, A. M. Sanchez, and P. S. Silva, "Thermo-mechanical analysis of an ITER ECH&CD upper launcher mirror," *Fusion Eng. Des.*, vol. 136, pp. 766–770, Nov. 2018.

[20] A. M. Sanchez et al., "Fluid-dynamic and thermo-mechanical analyses of the ITER electron cyclotron Miter bend mirror for the off-centered beam scenario," *Fusion Eng. Des.*, vol. 192, 2023, Art. no. 113643, doi: 10.1016/j.fusengdes.2023.113643.

[21] M. Vagnoni, R. Chavan, A. M. Sanchez, T. P. Goodman, and P. S. Silva, "Design concept and thermal–mechanical analysis of the optical mirror (M3) for the ITER ECH upper launcher," *IEEE Trans. Plasma Sci.*, vol. 48, no. 6, pp. 1543–1548, Jun. 2020.

[22] F. Sanchez, R. Bertizzolo, R. Chavan, A. Collazos, M. Henderson, and J. D. Landis, "Design and manufacturing of the ITER ECRH upper launcher mirrors," *Fusion Eng. Des.*, vol. 84, nos. 7–11, pp. 1702–1707, Jun. 2009.

[23] P. Santos Silva, R. Chavan, T. P. Goodman, A. M. Sanchez, and M. Vagnoni, "Design concept and thermal-structural analysis of a high power reflective mm-wave optical mirror (M2) for the ITER ECH-UL," *Fusion Eng. Des.*, vol. 146, pp. 618–621, Sep. 2019.

[24] L. Zhang et al., "A new design of launcher mirror for EAST electron cyclotron resonance heating system," *Fusion Eng. Des.*, vol. 173, Dec. 2021, Art. no. 112802.

[25] A. Allio et al., "Assessment of the performance of different cooling configurations for the launcher mirrors of the ECRH system of the DTT facility," *IEEE Trans. Plasma Sci.*, vol. 50, no. 11, pp. 4054–4059, Jul. 2022.

[26] K. Dutkowski, M. Kruzel, and K. Rokosz, "Review of the state-of-the-art uses of minimal surfaces in heat transfer," *Energies*, vol. 15, no. 21, p. 7994, Oct. 2022.

[27] G. Chouhan and G. Bala Murali, "Designs, advancements, and applications of three-dimensional printed gyroid structures: A review," *Proc. Inst. Mech. Eng., E, J. Process Mech. Eng.*, vol. 238, no. 2, pp. 965–987, Apr. 2024.

[28] E. R. Neovius, "Bestimmung zweier speciellen periodischen Minimalflächen, auf welchen unendlich viele gerade Linien und unendlich viele Ebene geodätische Linien liegen," Tech. Rep., 1883.

[29] O. Al-Ketan, M. Ali, M. Khalil, R. Rowshan, K. A. Khan, and R. K. A. Al-Rub, "Forced convection computational fluid dynamics analysis of architected and three-dimensional printable heat sinks based on triply periodic minimal surfaces," *J. Thermal Sci. Eng. Appl.*, vol. 13, pp. 1–33, May 2020, doi: 10.1115/1.4047385.

[30] M. Khalil, M. I. H. Ali, K. A. Khan, and R. A. Al-Rub, "Forced convection heat transfer in heat sinks with topologies based on triply periodic minimal surfaces," *Case Stud. Thermal Eng.*, vol. 38, Oct. 2022, Art. no. 102313.
[31] W. Tang et al., "Analysis on the convective heat transfer process and performance evaluation of triply periodic minimal surface (TPMS) based on diamond, gyroid and IWP," *Int. J. Heat Mass Transf.*, vol. 201, Feb. 2023, Art. no. 123642.
[32] Y. AlWeqayyan, E. Dasinor, B. Obeng, A. Abbas, and P. Phelan, "Experimental and simulated thermal resistance of thermogalvanic cells with triply periodic minimal surface structures," *Int. J. Thermal Sci.*, vol. 192, Oct. 2023, Art. no. 108430.
[33] V. Candela et al., "Laser powder bed fusion of CuCrZr for nuclear fusion acceleration components," in *Proc. 14th Int. Part. Accel. Conf.*, Geneva, Switzerland, 2023, p. 4896.
[34] *Simcenter STAR-CCM+*. Accessed: Jan. 20, 2024. [Online]. Available: https://www.plm.automation.siemens.com/global/it/products/simcenter/STAR-CCM.html
[35] *Next-Generation Engineering Design Software | NTopology*. Accessed: Jan. 20, 2024. [Online]. Available: https://ntopology.com/
[36] *Ansys Mechanical | Structural FEA Analysis Software*. Accessed: Jan. 20, 2024. [Online]. Available: https://www.ansys.com/products/structures/ansys-mechanical
[37] J. Öijerholm, C. Harrington, P. Gillén, A. Harte, L. Volpe, and J.-H. You, "Assessment of flow-assisted corrosion rate of copper alloy cooling tube for application in fusion reactors," *Nucl. Mater. Energy*, vol. 35, Jun. 2023, Art. no. 101433.

Eleonora Gajetti received the M.Sc. degree (cum laude) in energy and nuclear engineering (specialization: sustainable nuclear energy) from the Politecnico di Torino, Turin, Italy, in 2022, where she is currently pursuing the Ph.D. degree in energetics, with a focus on the development of advanced cooling systems for high-flux nuclear fusion components. During the M.Sc., she carried out an internship at Thales Electron Devices, Vélizy-Villacoublay, France, related to gyrotron cooling systems.

Massimiliano Bonesso, photograph and biography not available at the time of publication.

Alessandro Bruschi, photograph and biography not available at the time of publication.

Francesco Fanale, photograph and biography not available at the time of publication.

Saul Garavaglia, photograph and biography not available at the time of publication.

Gustavo Granucci, photograph and biography not available at the time of publication.

Alessandro Moro, photograph and biography not available at the time of publication.

Adriano Pepato, photograph and biography not available at the time of publication.

Afra Romano, photograph and biography not available at the time of publication.

Laura Savoldi (Member, IEEE) received the M.Sc. degree (cum laude) in nuclear engineering and the Ph.D. degree in energetics from Politecnico di Torino, Turin, Italy, in 1997 and 2001, respectively.

She is currently a Full Professor of nuclear plants with Politecnico di Torino. Her research interests are in the development, validation, and application of computational tools for the analysis of thermal-hydraulic transients in advanced heat transfer problems, including superconducting magnets and high heat flux components. In this frame, she developed the 4C code for the analysis of thermal-hydraulic transients in superconducting cables, coils, and related cryogenic circuits. She coauthored more than 200 papers published in international journals and proceedings of international conferences.

Prof. Savoldi serves as a referee for several international journals and conferences of her field of research, among which IEEE TRANSACTIONS ON APPLIED SUPERCONDUCTIVITY and IEEE TRANSACTIONS ON PLASMA SCIENCE.

Open Access funding provided by 'Politecnico di Torino' within the CRUI CARE Agreement